Biocompatible, multiresponsive nanogel composites for co-delivery of anti-angiogenic and chemotherapeutic agents

Malte S. Strozyk,[†,ǂ] Susana Carregal-Romero,[†]

Malou Henriksen-Lacey[†,//], Mathias Brust[ǂ], Luis M. Liz-Marzán*[,†,‡,//]

[†]Bionanoplasmonics Laboratory, CIC biomaGUNE, Paseo de Miramón 182, 20014 Donostia-San Sebastián, Spain

[ǂ]Department of Chemistry, University of Liverpool, Liverpool L69 7ZD, United Kingdom

[‡]Ikerbasque, Basque Foundation for Science, 48013 Bilbao, Spain

[//]CIBER de Bioingeniería, Biomateriales y Nanomedicina, CIBER-BBN, 20014 Donostia-San Sebastián, Spain

*e-mail: llizmarzan@cicbiomagune.es

ABSTRACT

Single therapy approaches are usually insufficient to treat certain diseases, due to genetic differences between patients or disease resistance. Therefore, such approaches are gradually replaced by combination therapies comprising two or more drugs. In oncology these include BRAF inhibitors, cytotoxic, anti-angiogenic or immunomodulatory agents, among others. We propose herein the use of multiresponsive nanogel composites for the co-delivery of a DNA intercalator (doxorubicin) and an anti-angiogenic and immunomodulatory agent (pomalidomide). We introduce a surfactant-free synthetic protocol to decorate biocompatible poly(ethylene glycol)methacrylate nanogels (PEGMA) with evenly distributed gold

nanoparticles and explore their ability to deliver drugs upon stimulation by various triggers such as heat, light and reducing agents present in the intracellular environment. We further demonstrate that an additional polymer coating on the nanogel surface can decrease uncontrolled drug leakage, and modulate cellular uptake and the drug release profile.

INTRODUCTION

Chemotherapy still prevails as the most common treatment for cancer. However, there is a rising demand for alternative therapies, which involve the use of anticancer drugs combined with other molecularly target agents toward the reduction of side effects and the enhancement of the treatment efficacy.[1,2] The use of nanoparticles (NPs) for drug delivery is a well recognized method to control the delivery kinetics and biodistribution of the drug in question, as well as offering protection from biological conditions which can cause drug degradation.[3–7] Furthermore, NP materials need not be limited to one sole material or be loaded with a single drug. In fact, this leads to many possibilities in terms of triggered, controlled, drug release and co-delivery that can be combined with multimodal imaging.[8–11] Regarding chemotherapy, NPs offer the possibility to improve treatment efficacy by delivering cytotoxic drugs to cancerous cells with minimal exposure to non-cancerous cells, thereby avoiding chemotherapy side effects.[12–15] Tumors, however, are complex structures and their growth promotes angiogenesis in an autocrine manner, thereby allowing a constant supply of nutrients and oxygen to the cancerous cells.[16–18] The suppression of tumor growth by action of anti-angiogenic agents is therefore an appealing method to target cancer.[19,20] One of the most interesting aspects therefore of NPs is their ability to deliver a combination of drugs which can target different aspects of tumour growth and persistence. One such example of this is Doxil, a liposomal doxorubicin carrying NP system, which has been combined with dexamethasone and pomalidomide and is currently in clinical trials to treat Multiple Melanoma (MM) cancer (NCT01541332 from www.clinical trials.gov).

In this context, we propose the use of nanogels for combination therapy and controlled release of drugs. Nanogels are formed by crosslinked polymeric networks that possess a

large water content and open spaces with a characteristic mesh size. The mesh size governs the diffusion of drugs within the nanogel and the chemical interaction between the polymer structure determines the drug entrapment efficiency.[21,22] Nanogels show several advantages over other drug carrier systems, which are related with the mild conditions of drug encapsulation, which allow entrapment of labile drugs (hydrophilic and hydrophobic), their excellent biocompatibility and the easy tailoring of their responsiveness toward triggers of drug release.[23,24] In contrast, the main drawback is the uncontrolled leakage of drugs. The nanogel polymer chemistry can be designed to release cargo molecules upon different stimuli such as e.g. pH or heat.[25] By including gold (Au) NPs within the nanogel, near-infrared (NIR) illumination can be used to induce local heating at the AuNP surface, thereby providing a further trigger for drug release and offering NP-based hyperthermia.[26,27] Importantly, the use of NIR illumination renders such a system suitable for use in biological tissues, due to the reduced absorption by tissue of light with wavelength between 650 and 950 nm.[28]

In this proof of concept work we demonstrate that AuNP-containing thermosensitive nanogels, coated with an appropriate polyelectrolyte, are suitable platforms for the co-delivery of doxorubicin (Doxo) – a cytotoxic agent and DNA intercalator – and pomalidomide (Poma) – an anti-angiogenic and immunomodulatory agent.[29–31] These drug delivery systems are preferentially cytotoxic to cancer cells *in vitro*, while also being efficient at inhibiting angiogenesis in tube-formation assays *in vitro*. Nanogels are a highly versatile system in which drug release profiles can be controlled *via* polyelectrolyte coating and/or various external stimuli, showing good biocompatibility and biodegradation *in vitro.* The final nanogels thus offer a stable platform that can be prepared by straightforward

production methods and used to deliver several drugs, with both hyperthermia and photothermal ablation therapy characteristics.

RESULTS AND DISCUSSION

Formation of polyelectrolyte coated AuNP decorated PEGMA nanogels

The thermoresponsive nanogels used for the loading and co-delivery of the two selected drugs were based on poly(ethylene glycol) methyl ether methacrylate (PEGMA), and formed by the well-established free radical polymerization method.[32–34] PEGMA nanogels were chosen because of their easy-to-tailor lower critical solution temperature (LCST), ranging from room temperature up to 90 ºC,[35,36] and because their monomer constituents are non-toxic.[37] These are two major advantages, as compared *e.g.* to the widely used poly(N-isopropyl acrylamide) (pNIPAM).[38,39] In the second step of the synthesis, a surfactant-free method was used to incorporate light responsive (plasmonic) AuNPs within the PEGMA nanogels, thereby avoiding potential toxicity of surfactants and keeping the AuNPs surface free to adsorb other molecules (**Figure 1a**). To this purpose, pre-made nanogels were immersed in a solution of $HAuCl_4$, followed by addition of a strong reducing agent, $NaBH_4$. The amino groups in the nanogels (present in the monomer 2-aminoethyl methacrylate hydrochloride) coordinate the gold precursor and small gold seeds of approximately 3 nm were formed upon $NaBH_4$ reduction. These seeds were subsequently grown by addition of $HAuCl_4$, sodium bromide and formaldehyde, which displays a pH-dependent reducing potential.[40] Sodium bromide helped in controlling AuNP growth due to the formation of a gold bromide complex with higher stability as compared to free $HAuCl_4$. When the process was carried out, in the absence of either Au seeds or sodium bromide, nanogels were obtained with particle

disparity, anisotropy and aggregation (**Figure S1**, Supporting Information). On the contrary, seeded growth produced nanogels with evenly distributed AuNPs with an average size of 23.2 ± 6.1 nm and a low proportion of anisotropic particles (**Figure 1b**). The nanogel containing AuNPs displayed a localized surface plasmon resonance (LSPR) band centered at 540 nm (**Figure 1c**), which is redshifted with respect to free AuNPs with similar sizes due to some anisotropy and plasmon coupling between the AuNPs in the gel. This two-step process allows a good level of control over the final AuNP size, which can range from 9 to 30 nm simply by tuning the amount of Au seed-loaded nanogels added to the growth solution (**Figure S2**). PEGMA nanogels were subsequently wrapped with biodegradable and biocompatible polyelectrolytes to modify the release profile of encapsulated drugs, and to add a coating that can easily bind other functional moieties (such as antibodies or dyes) for future applications.[41] Functionalization was carried out by immersing AuNP-loaded nanogels in the appropriate polyelectrolyte solution followed by several washing steps to remove non-adsorbed polyelectrolytes. Samples with different surface compositions were named as follows: 1) AuNG1 had no coating, 2) AuNG2 was coated with poly-L-arginine and 3) AuNG3 was coated with polyalginate. We studied the influence of the two different coatings, *i.e.* the polypeptide poly-L-arginine and the polysaccharide polyalginate, on the physicochemical properties of the nanogels, and their drug loading and release profiles for both Doxo and Poma.

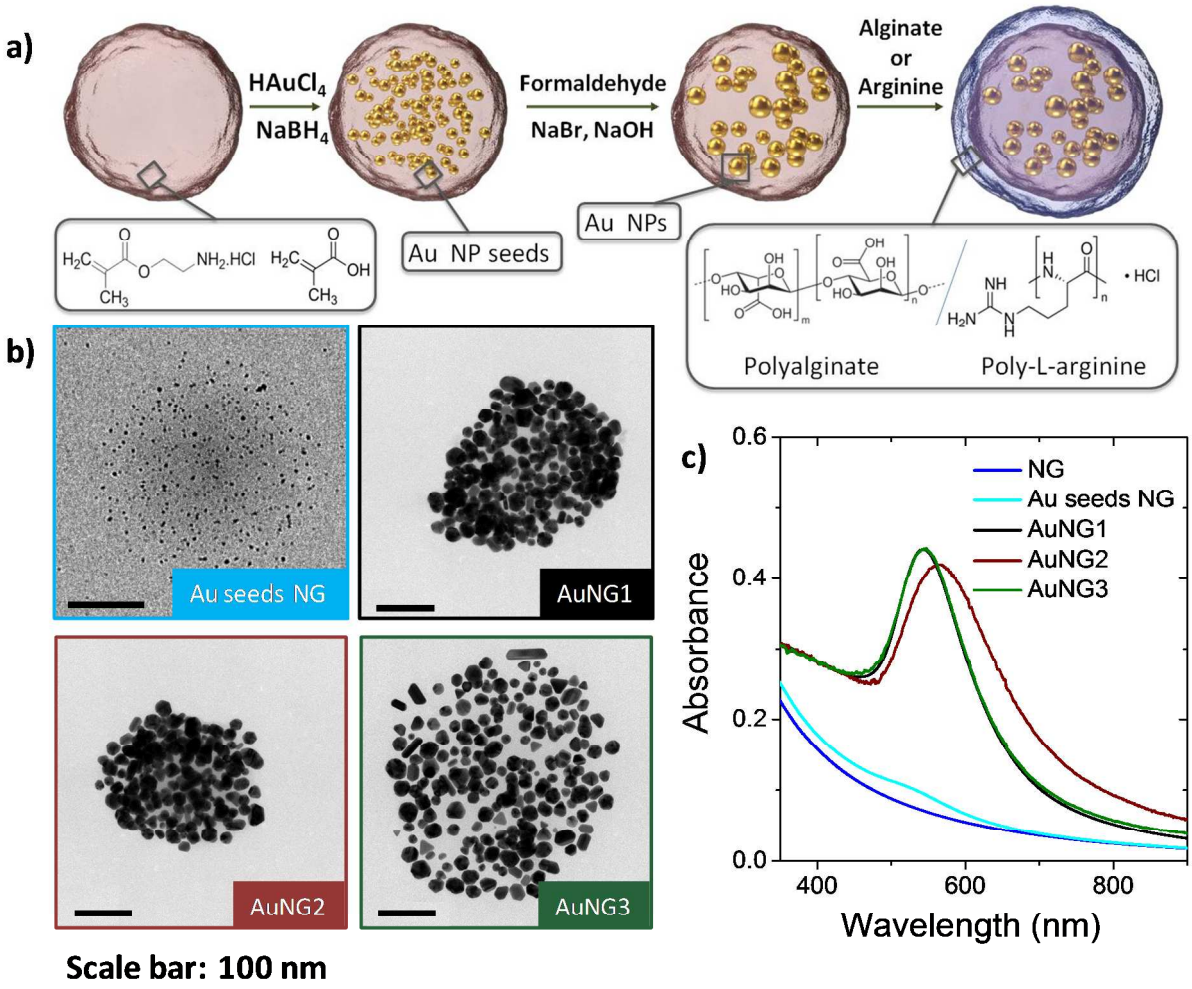

Figure 1. a) Schematic representation of the in-situ growth of gold nanoparticles in PEGMA nanogels. Small gold seeds were synthesized by reduction with $NaBH_4$. Further growth was realized by introducing the nanogels with seeds in a growth solution containing NaBr and formaldehyde at high pH. The obtained nanogels were finally wrapped with a layer of polyelectrolyte. b) Representative TEM pictures of the nanogels during the different growth steps, as labeled. c) UV-Vis spectra of the corresponding particle colloids.

Influence of polyelectrolyte coatings on the physicochemical properties of PEGMA nanogels

The presence of the polyelectrolytes on PEGMA nanogels was confirmed by X-ray photoelectron spectroscopy (XPS), zeta potential, LSPR and particle size analysis. XPS data showed a clear decrease in the amount of Au on the nanogel surface between coated and non-coated nanogels. Additionally, nitrogen was identified in sample AuNG2 due to

the amino groups in poly-L-arginine, whereas AuNG3 showed a higher amount of oxygen due to the hydroxyl and carboxyl groups in polyalginate, as compared with AuNG1. Changes in zeta potential, LSPR and particle size were also observed, as shown in **Table 1**. AuNG2 was found to become more compact upon polyelectrolyte addition, which in turn reduced the AuNP interparticle distance inside the nanogels, resulting in stronger plasmon coupling and a LSPR red shift of 23 nm after functionalization (**Figure 1b,c**). The decrease in overall nanogel size observed in AuNG2 is due to the strong electrostatic interaction between the negatively charged nanogel and the positively charged polyelectrolyte, which results in the formation of a polyelectrolyte-gel complex.[42] It has been reported that, if the molecular weight of the coating molecules is low enough they can even penetrate the nanogel reducing the mesh size.[43] In contrast, functionalization with the anionic polyalginate did not modify the LSPR but caused slight swelling of the nanogel, presumably due to the weaker interactions between polyalginate and the nanogel.

Table 1. Differences in elemental composition, LSPR, zeta potential (ζ) and hydrodynamic diameter (D_h) of the coated and non-coated PEGMA nanogels.

Sample	N (at.%)	C (at.%)	O (at.%)	Au (at.%)	LSPR (nm)	ζ (mV)	D_h (nm)
AuNG1	0	64.3	24.8	10.9	544	-36.2 ± 0.2	274.1 ± 2.0
AuNG2	11.1	56.3	27	5.6	567	40.9 ± 0.3	223.8 ± 1.4
AuNG3	0	46.9	49.6	3.5	544	-34.5 ± 0.8	292.1 ± 4.4

In the context of physicochemical changes, it is worth highlighting the strong influence of polyelectrolyte coatings on the thermoresponsive behavior of PEGMA nanogels. Bare nanogels displayed a LCST above 30 ºC (**Figure S11**) and the inclusion of AuNPs inside the nanogels did not hinder their ability to shrink or swell in response to heat changes (**Figure 2a**). In contrast, we noted significant differences in the swelling ratios (Q)

depending on the type of polyelectrolyte coatings. Q was defined as the ratio between the volume of the corresponding nanogel at a temperature T versus the volume at 70 ºC (Q=V(T)/V(70 ºC)). **Figure 2b** illustrates the observed decrease in Q for coated PEGMA nanogels. The largest decrease of Q between coated and non coated nanogels was observed for AuNG2, which almost completely lost its thermoresponsiveness. This result is in agreement with the reduction in particle size upon coating with poly-L-arginine. Interestingly, the LCST increased from 32 ºC in AuNG1 to 36 ºC and 37 ºC for AuNG2 and AuNG3 respectively, closer to physiologically relevant temperatures.

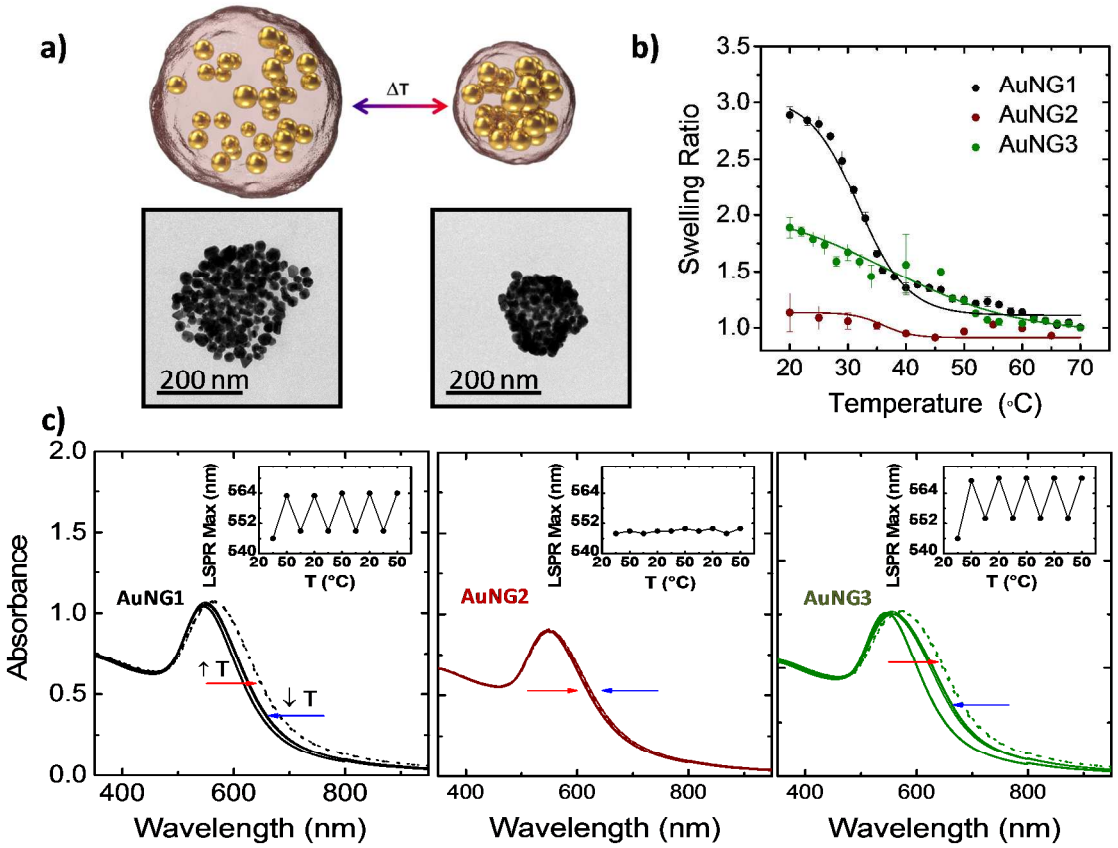

Figure 2. a) Schematic representation of the shrinking process and representative TEM pictures in collapsed and swollen states. b) Dynamic light scattering monitoring of the swelling ratio in AuNGs. c) UV-Vis spectra of the nanogels, alternating at 20 ºC and 50 ºC, plotted as solid and dashed lines, respectively. The insets show the LSPR maxima during each cycle.

These results were confirmed with UV-Vis spectroscopy. As expected, the thermoresponsive decrease in the volume of the nanogel led to smaller inter-particle distances and hence to a red shift and broadening of the LSPR band. AuNG1 and AuNG3 behave similarly, with an approximate red shift of 14 nm between 20 and 50 ºC. We verified the reversibility of the shift by carrying out multiple heating/cooling cycles. The shift was fully reversible over 5 temperature cycles (**Figure 2c, inset**). AuNG2, in contrast, shows no change of the LSPR, in accordance with the low Q value (Q= 1.1). Interestingly, the thermoresponsive behavior of coated PEGMA nanogels was observed to further change after encapsulation of drugs, in such a way that AuNG2 recovered its thermal responsiveness (**Figure 3a**). Further detailed information about the thermal behavior of different formulations of PEGMA nanogels has been included in the Supporting Information.

In addition to the described physicochemical differences, the colloidal stability between coated and non-coated PEGMA nanogels was studied by incubating them in different media of biological interest and analyzing the corresponding values of LSPR maxima and zeta potential.[44] AuNG3 displayed higher colloidal stability in non-supplemented cell culture media as compared with AuNG1 and AuNG2, which aggregated due to the high ionic strength, as previously reported for different polymer coated AuNPs. All PEGMA nanogels showed colloidal stability in cell culture media supplemented with serum due to protein adsorption (data shown in the Supporting Information).[45]

Influence of polyelectrolyte coatings on stimulated drug delivery

Drug loading was achieved by immersing AuNP decorated PEGMA nanogels in an aqueous solution of drugs in basic conditions, and quantified by the decrease of drug

concentration in solution after loading. The maximum loading of Doxo was 0.33 mol/mg(Au) for AuNG1 and AuNG3, and 0.30 mol/mg(Au) for AuNG2. The encapsulation of Poma was less efficient with only 0.025 mol/mg(Au) for AuNG1, 0.019 mol/mg(Au) for AuNG2 and 0.020 mol/mg(Au) for AuNG3. For the sake of simplicity we discuss in the main text the loading and release behavior of Doxo alone, though a similar analysis was carried out for Poma and is discussed in the Supporting information. The entrapment of drugs was possible due to attractive interactions between Au decorated PEGMA nanogels and Poma and Doxo. Both electrostatic interactions and hydrogen bonding may be involved in the loading of the nanogels, due to the presence of carbonyl and ester groups in the nanogel and amino groups in both drugs.[46] In fact, a change in the zeta potential of the nanogels toward more positive values after drug encapsulation was observed, as previously reported for similar nanogels.[47] **Figure 3** shows the influence of polyelectrolyte presence on Doxo release from PEGMA nanogels, as a function of increasing temperature. Both polyelectrolytes shifted the thermal release to temperatures above 37 ºC, as compared to the non-coated AuNG1 (**Figure 3a**). However, poly-L-arginine (AuNG2) hindered more the uncontrolled leakage of Doxo from the nanogel compared to polyalginate (AuNG3), but also made PEGMA nanogels less efficient at thermally triggered release. **Figure 3b** shows an 18-fold increase for AuNG3 but only a 5-fold increase for AuNG2, of released Doxo between room temperature and 50 ºC.

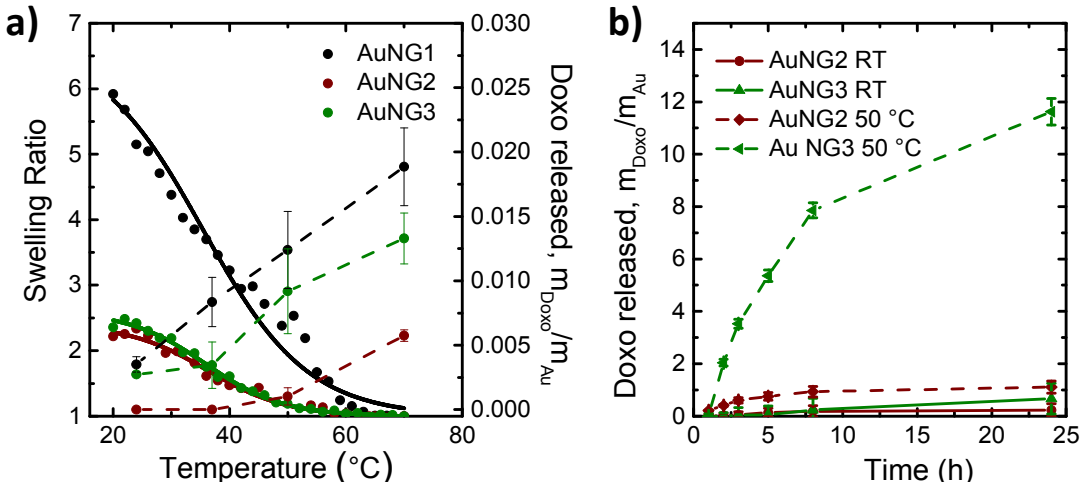

Figure 3. a) Dynamic light scattering measurements showing the correlation between the decrease in the swelling ratio (solid lines) of AuNG1, AuNG2 and AuNG3 and the increase in Doxo release (dashed lines) with the increase of temperature. b) Cumulative Doxo release over time at room temperature (solid lines) and at 50 ºC (dashed lines).

Near-infrared (NIR) light, glutathione (GSH) and pH were also confirmed to trigger the release of drugs from AuNP decorated PEGMA nanogels, *via* different mechanisms (**Figure 4a-c**). The interaction of NIR light with AuNPs inside the nanogels led to shrinkage and in turn remotely controlled release of drugs due to the photothermal effect. Upon continuous NIR illumination (808 nm, 8.3 W/cm^2), an initial increase in both the recorded temperature and Doxo release were noted, followed by a plateau in both measurements after ca. 10 minutes (**Figure 4a**).

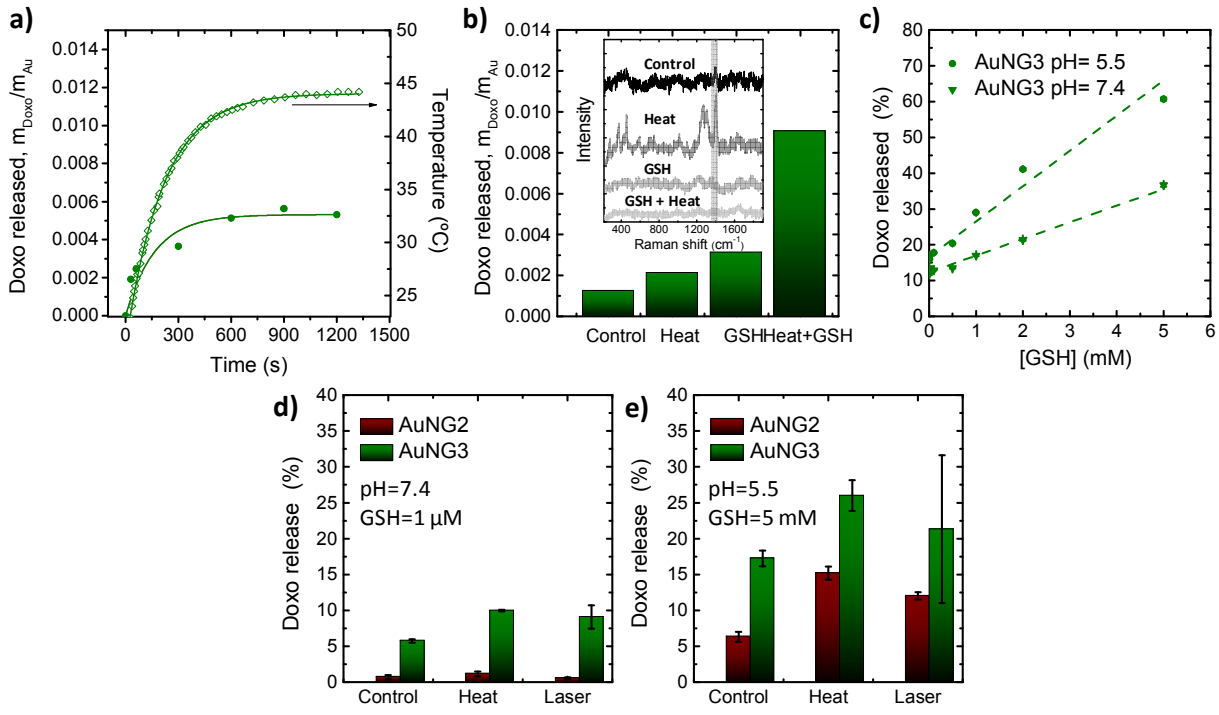

Figure 4. a) Temperature increase (open circles) of AuNG3 solution under NIR illumination (808 nm, 8.03 W/cm^2) and the corresponding doxorubicin release (filled circles). b) Doxo release from AuNG3 upon heating and/or GSH addition and corresponding SERS spectra (inset). SERS spectra were recorded in solution at a concentration of 5 µg/mL(Au), P_{laser}= 12mW for 633 nm and t_{int}=20s with a 10x objective (NA=0.35). The assigned band at 1420 cm^{-1} is highlighted with a grey background. c) pH influence on the release of Doxo at different [GSH]. d,e) Summary of the different Doxo release efficiencies comparing the delivery at room temperature (control) versus the delivery upon the application of external stimuli, NIR light and heat (50 ºC) in solutions mimicking the extracellular (d) and intracellular environment (e).

The mechanism of drug release triggered by heating (including NIR light irradiation) and subsequent nanogel shrinkage can be related to the removal of hydrogen bonding between the drugs and the nanogel itself, but also to the decrease in the radius of the nanogel and shortening of the diffusion path for entrapped drugs. In contrast, drugs that are released through reduced temperature induced swelling of nanogels have been shown to diffuse faster when the mesh size of the hydrogel increases due to hydrogen bonding with water molecules.[48,49] It should be noted that, realistically, the required temperature decrease is hard to achieve in biological systems. The release mechanism of Doxo and Poma at different temperatures from AuNG2 and AuNG3 was analyzed using the semi-empirical

Peppas model,[50] obtaining in both cases values of the release exponent *n* corresponding to the anomalous transport regime ($0.43<n<0.85$), which represents a mixture between diffusion-controlled release and other mechanisms (see Supporting Information).

GSH was also found to enhance drug release from AuNP decorated PEGMA nanogels. This trigger is of interest for intracellular drug delivery since its concentration is over 200 fold higher within cells (0.2-10 mM) than in the extracellular environment (2-20 μM).[51,52] To compare the GSH triggered Doxo release with that induced by heating, we exploited the ability of AuNPs to induce surface enhanced Raman scattering (SERS). SERS was used to identify Doxo within the AuNG3 nanogel after incubation with GSH, after heating and after both heating and GSH incubation, and the signals were compared to the corresponding fluorescence intensity of Doxo delivered to the supernatant from the nanogel. **Figure 4b** shows that both GSH and heat triggered the release of Doxo from the nanogel, and both triggers, acting in synergy, released 1.8 times more than the sum of the two triggers separately (30 min incubation time, T= 50 °C, [GSH]= 5 mM). The presence of Doxo was monitored using the characteristic SERS peak at 1420 cm^{-1} (corresponding to the C-O-H and C-H bending mode). The temperature increase enhanced the signal of Doxo as compared with the control experiment at room temperature, due to shortening of the inter-particle distances, which is known to induce a further enhancement of the Raman signal. However, upon application of both T increase and GSH, the Doxo signal vanished faster than by only heating. The release mechanism of GSH could be related to ion displacement,[23] since it is known that GSH adsorbs onto AuNPs and polymers and can trigger this kind of release mechanism intracellularly.[53,54] In addition, we observed degradation and disassembly of the Au decorated PEGMA nanogels, both after GSH

exposure in solution and in *in vitro* experiments, which would subsequently enhance drug release (Supporting Information).

pH changes affect hydrogen bonding,[55] as well as charges on amino and carboxylic groups in the nanogels. As pH is also known to considerably decrease during the endocytotic pathway in cells, we studied the effect of pH on the release of Doxo from the nanogels. By exposing AuNG3 to pH 7.4 or pH 5.5, values that are representative of the extracellular and intracellular environment respectively, we noted a 2-fold increase in Doxo release. Additionally, the increased Doxo release at low pH was more pronounced in the presence of GSH at the usual concentrations in the intracellular environment (**Figure 4c**). We subsequently compared how all the aforementioned triggers can affect drug release in an environment mimicking both extracellular and intracellular conditions. **Figure 4d**,**e** shows that intracellular conditions enhance Doxo release induced by both heat and NIR illumination. Moreover, the polyelectrolytes on the nanogels surface caused significantly different drug release profiles, AuNG2 being more efficient in avoiding drug leakage, whereas all triggers enhanced drug release from AuNG3. We therefore conclude that AuNG3 appears to release higher amounts of Doxo, yet AuNG2 releases the same drug in a more controlled way under the effect of different triggers (**Figure S14**). A similar study was carried out for the release of Poma (**Figure S14**). In this case, release was more significantly affected at intracellular conditions (high [GSH] and low pH) than by the application of external stimuli. AuNG2 were more efficient in releasing Poma than AuNG3 and uncontrolled leakage was similar for both types of nanogels. The different release profiles shown in our work are key when selecting the appropriate carrier for a specific drug that could demand a faster release or which is very toxic and should be only released at the target cells.

Modulation of cellular uptake *in vitro*

Polyelectrolyte shells on AuNG2 (poly-L-arginine) and AuNG3 (polyalginate) were shown to affect nanogel uptake by both cancer and non-cancer cells, due to the different composition and surface charge of the nanogels. Taking into consideration that the increased metabolic activity of cancer cells compared with non-cancer cells can be exploited to improve nanogel uptake,[56–58] we conducted a co-culture of HeLa cancer cells with healthy human dermal fibroblasts (HDF) to determine the differences in nanogel endocytosis. Using fluorescence microscopy and TEM we observed higher levels of endocytosis for AuNG2, as compared to AuNG3 (**Figure 5**). Flow cytometry determined the levels of AuNG2 and AuNG3 uptake in this co-culture, measured 24 h after a short 2 h incubation. The percentages of HDF cells positive for Doxo (used as a fluorescent label) were 75.6% and 33.7% for AuNG2 and AuNG3 nanogels, respectively, whereas the percentage of HeLa cells positive for Doxo were 99.4% and 75.6% for AuNG2 and AuNG3, respectively. This shows significant differences in cell specificity which can indeed be ascribed to the enhanced metabolic rates of cancer cells, as well as increased levels of AuNG2 uptake compared to AuNG3, due to the overall cationic charge of the AuNG2 system. Cationic nanoparticles and also molecules with overall positive charges (e.g. cell penetrating peptides) are well known to associate with cell membranes to higher levels than their anionic counterparts. As expected, incubation of cells (both cancerous and healthy) with free Doxo resulted in rapid nuclear localization, whereas Doxo containing AuNG2 and AuNG3 were localized in endosomes (**Figure 5a,b**). Similar results were obtained with breast cancer MCF-7 cells (**Figure S19**), in agreement with previous

studies.[56] However, such increased levels of uptake in cancer cells did not correlate with higher drug release *in vitro* (**Figure 6**).

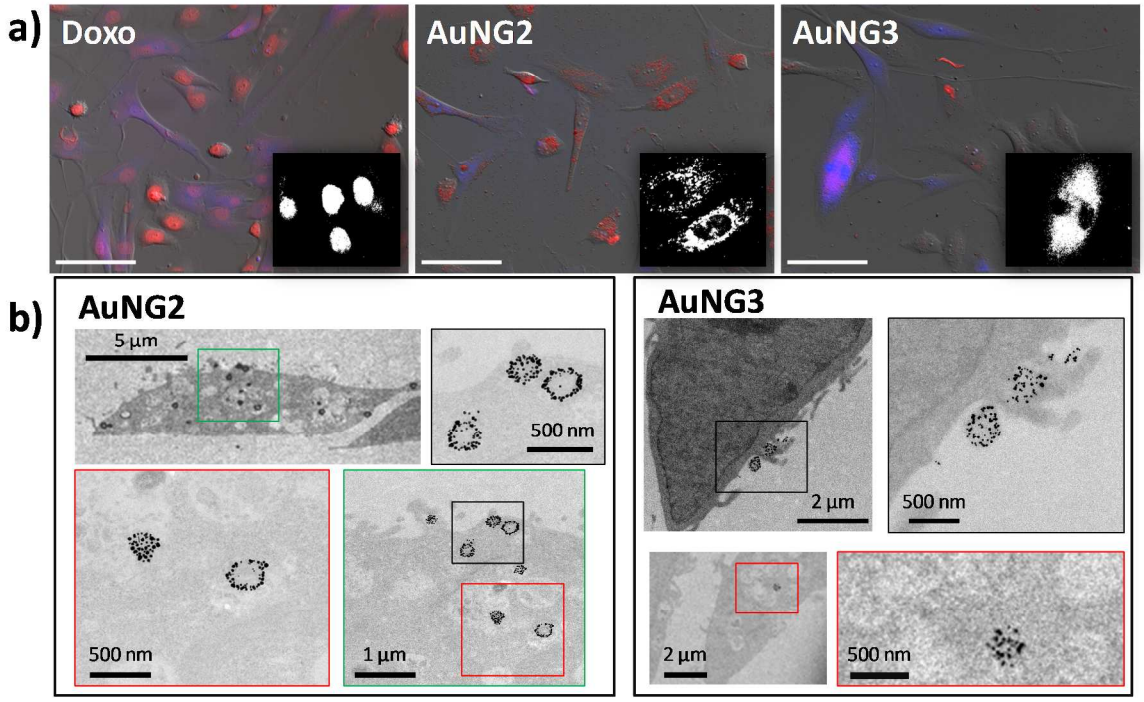

Figure 5. a) Cellular uptake of free Doxo, AuNG2 and AuNG3 nanogels. A co-culture of HeLa (unstained) and HDF (blue stained) cells were exposed to Doxo and Doxo containing AuNG2 and AuNG3 for 2 h and uptake visualized using Doxo fluorescence (shown in red in main images or in white in inserts for clarity). Clear nuclear (left image) or endosomal staining (middle and right images) is seen after free or nanogel delivered Doxo, respectively. Scale bars are 100 µm. b) TEM images of HeLa cells exposed to AuNG2 and AuNG3 for 2 h and then processed the following day for TEM imaging. Magnified photos are shown in color coded boxes.

Modulation of co-delivery *in vitro*

The effect of the two drugs Poma and Doxo was measured separately because they affect cells through different molecular mechanisms. We first verified that the increased levels of AuNG-PEGMA nanogel uptake by cancer cells compared to non-cancer cells resulted in downstream cell death. As seen in **Figure 6a**, whilst free Doxo resulted in cell death of both cancer and non-cancer cells in the co-culture system, exposure to Doxo-containing AuNG2 and AuNG3 caused predominate cytotoxicity to cancerous HeLa cells whilst HDF cells remained viable. The presence of Poma within the nanogels was verified as not

inducing any cytotoxic effects (**Figure S20**). The high levels of cytotoxicity noted in HeLa cells was slow, occurring ca. 4 days after the initial exposure of the cells to the AuNG-PEGMA nanogels. We subsequently investigated the use of NIR light as a method to improve Doxo release and subsequent cell death, compared to non-illuminated controls. NIR-light illumination of HeLa cells incubated with AuNG-PEGMA nanogels resulted in a significant decrease in the viability over the non-illuminated cells (**Figure 6b**). Non-Doxo loaded nanogels (AuNG*) were used as second control, showing that it was possible to induce hyperthermia with AuNP-PEGMA nanogels, which is interesting for combined therapy as previously reported for other drug delivery systems.[59] However, we verified that there exists an enhancement of Doxo release under NIR light illumination *in vitro* when lower power densities are applied, thereby avoiding hyperthermia (**Figure S21**).

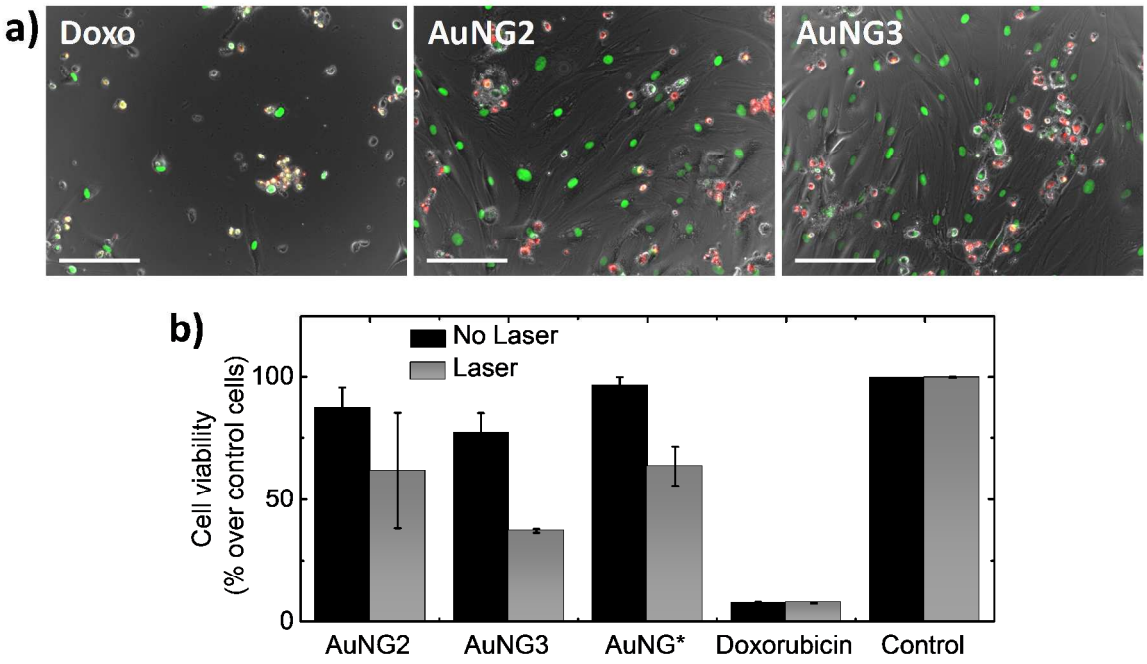

Figure 6. a) Live/Dead staining of HeLa/HDF co-cultures, ca. 4 days post initial exposure to free Doxo, or Doxo-containing AuNG2 and AuNG3. Live cells show green-channel fluorescence whilst dead cells uptake propidium iodide and are positive for red channel fluorescence. The predominant live population (green) are HDF cells which can be identified by their characteristic shape, whereas HeLa cells are the majority "dead" population. Scale bars are 200 µm. b) NIR-laser induced hyperthermia and photo-thermal-induced cytotoxicity of HeLa cells. HeLa cells were exposed to Doxo-containing AuNG2 and AuNG3, or non-Doxo control nanogels (AuNG*) for ca. 12h, followed by illumination with an

808 nm diode laser at 16 W/cm^2 for 20 minutes. Cell viability was measured the following day using the MTT assay (mean of triplicate wells +- SD).

The drug Poma has been shown to be highly efficient at inhibiting angiogenesis,[31] in addition to a wide variety of immune system modifying effects such as the inhibition of cytokine production in LPS-stimulated peripheral blood mononuclear cells (PBMCs),[60] thereby placing it in the group of immunomodulatory drugs (IMiDs).[61] We took advantage of these immunomodulatory effects as a method to verify that Poma remained active after release from AuNG nanogels. In order to do so, we exposed LPS-stimulated J774 murine monocyte-macrophage cells to AuNG2 and AuNG3, containing Poma alone or Doxo and Poma, and determined the levels of IL-6 cytokine produced. Compared to non-exposed controls, IL-6 levels were reduced by 90%, similar to exposure to free Poma (**Figure S22**). No significant differences in the ability of AuNG2 and AuNG3 to inhibit LPS-induced IL-6 were observed, nor did the presence of Doxo in the formulations hinder Poma. We next investigated the ability of Poma containing nanogels to inhibit angiogenesis in an *in vitro* tube formation model. Due to the short time span of the assay ("tubes" form within hours and cells die naturally at approximately 24 h post planting), we pre-incubated HUVEC cells with Poma-containing nanogel formulations overnight, and the following day we planted the nanogel-containing HUVEC cells on the tube-inducing gel support. **Figure 7a** shows the effective inhibition of tube formation when healthy HUVEC cells, otherwise capable of tube formation, were pre-incubated with both Poma- containing AuNG2 or AuNG3, at a concentration equivalent to 10 μM. On the contrary, HUVEC cells pre-incubated with Au decorated PEGMA nanogels without Poma were able to form tubes (**Figure S23**), as expected. In addition to Poma effects on HUVEC cells when grown under angiogenesis-

stimulating conditions, the cell surface area and the aspect ratio (AR) of HUVEC cells were significantly reduced upon exposure to Poma-containing nanogels when grown under "normal" tissue culture conditions (**Figure 7b,c**). IMiD compounds have been shown to activate GTPases, enzymes which are responsible for cellular cytoskeleton reorganization, cellular differentiation and movement.[62] In fibroblasts, Poma has been shown to induce formation of actin stress fibers,[62] and changes of cell area and aspect ratio have been documented upon exposure of cells to both anti- and pro-angiogenic molecules.[63,64] Considering that the production of pro-angiogenic molecules such as VEGF and bFGF is inhibited by a cascade of signaling pathways due to pomalidomide's ability to down-regulate cell adhesion molecules and reduce VEGF, bFGF and IL-6 secretion,[65] it is reasonable to assume that Poma will affect cell surface area. Exposure of HUVEC cells to Poma-containing nanogels resulted in a decrease in cell size, reducing the surface area by 1/3 – 2/3 of the original value. The decrease in cell surface area and aspect ratio was more pronounced for Poma-containing AuNG2 than for AuNG3, which can be correlated with an enhanced cell uptake of these nanogels, but also with the higher degree of Poma release observed in solution. Interestingly, we did not observe any similar effects upon exposure of HUVEC cells to free Poma, which suggests that these IMiD mediated changes in cell morphology are highly dependent on exposure time and subsequent Poma release from nanogel formulations.

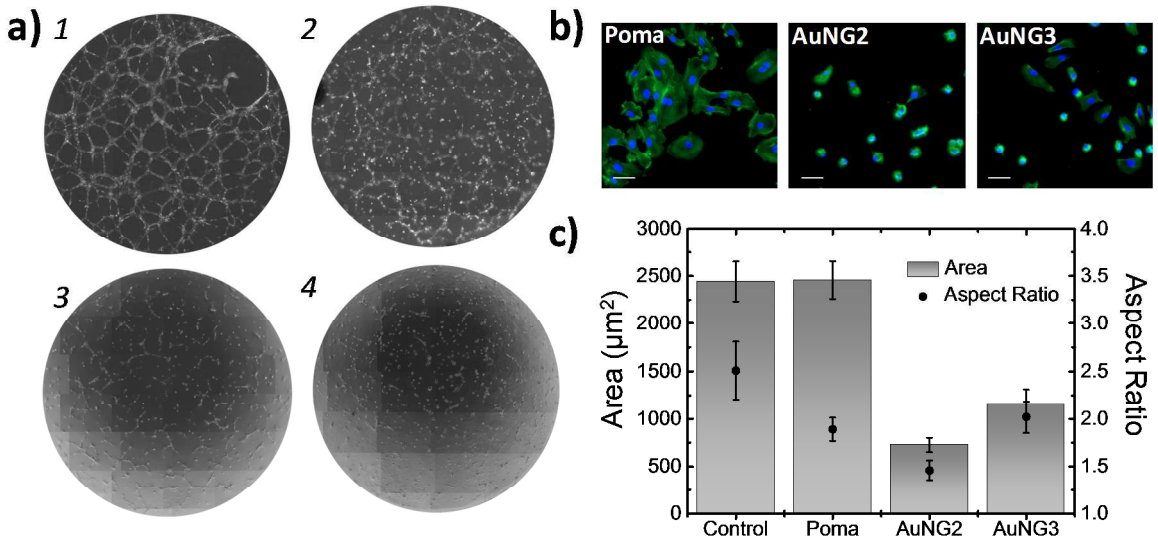

Figure 7. a) The angiogenesis tube formation assay shows the ability of HUVEC cells to grow vessel-like interconnecting networks through the aid of growth factors present in the underlying gel. In cases were no nanogels were applied (*1*), established tube formation is seen within 6 h, yet with HUVEC cells pre-incubated with AuNG2 (*3*), or AuNG3 (*4*), or HUVEC cells incubated with free pomalidomide (*2*), poor or no tube-formation is seen. Each image (circle) is 4 mm in diameter showing the whole well. b) HUVEC cells incubated with free Poma, AuNG2 or AuNG3 for 4 h at a final Poma concentration of 10 μM. Cells were washed, fixed and stained with Dapi and AF488-phalliodin to show the nucleus and actin fibers respectively. Scale bars are 50 μm. c) Area and aspect ratio (AR) of cells described in (b), measured using ImageJ from at least 30 cells from 3 separate images. Mean +- SD is shown.

CONCLUSIONS

In summary we synthesized a versatile multiresponsive drug delivery system based on thermoresponsive nanogels containing gold nanoparticles for the co-delivery of doxorubicin and pomalidomide. The gold nanoparticles inside the nanogel were synthesized in a new two-step method to ensure even particle distribution throughout the gel and surfactant-free synthesis. The leakage of drugs was reduced by wrapping the nanogels with a polyelectrolyte shell. We studied two possible coatings: polyalginate and poly-L-arginine. These two coatings produced different modifications in the thermoresponsive behavior of the nanogels and other physicochemical properties that were characterized and influenced first, the stimuli responsive release of the two drugs and

second, their interaction with cells and their drug delivery *in vitro* We showed that pH, glutathione concentration, heat and NIR-light can all trigger the release of drugs in an extent that was dependent on the chemical nature of the drug and the coating polyelectrolytes. Both coated nanogel systems showed enhanced uptake by cancer cells compared to non-cancer cells, due to their enhanced metabolism, but more specific uptake in cancer cells was seen for nanogels coated with positively charged polyalginate. Taking this into account and considering: 1) both polyelectrolyte coated PEGMA nanogels have low leakage and show a slow drug release profile, 2) the cytotoxic doxorubicin is released more efficiently by a remote controlled trigger (light) from AuNG3 than AuNG2 nanogels and 3) the release of pomalidomide was effective for the two nanogel formulations, we can conclude that polyalginate coated PEGMA nanogels can be considered as the more convenient drug delivery system for the remote controlled co-delivery of doxorubicin and pomalidomide.

METHODS

Materials. Milli-Q water (resistivity 18.2 MΩ·cm) was used in all experiments. Hydrogen tetrachloroaurate trihydrate ($HAuCl_4 \cdot 3H_2O$, ≥99.9%), di(ethylene glycol) methyl ether methacrylate, poly(ethylene glycol) methyl ether methacrylate, poly(ethylene glycol) diacrylate, 2-aminoethyl methacrylate hydrochloride, methacrylic acid, formaldehyde (37 wt%), doxorubicin hydrochloride and poly-L-arginine hydrochloride (mol wt >70,000) were all purchased from Sigma-Aldrich. Pomalidomode was purchased from Abcam.

Alginic acid (sodium salt) was obtained from Fisher Scientific. All glassware was washed with aqua regia, rinsed 3 times with Milli-Q water and dried before use.

Synthesis of poly ethylene glycol methacrylate nanogel.

Nanogels were synthesized by purging a 300 mL Milli-Q water solution of 5.6 g di(ethylene glycol) methyl ether methacrylate, 2,4 g poly(ethylene glycol) methyl ether methacrylate, 160 mg poly(ethylene glycol) diacrylate, 297 mg methacrylic acid and 576 mg 2-aminoethyl methacrylate hydrochloride with argon for an hour at 70 ºC. The reaction was then started by adding 120 mg of 2,2, azobis(2methylpropionamidine)dihydrochloride disolved in 2 mL of degassed Milli-Q water and run for 12 hours at 70 ºC.

Synthesis of AuNP decorated nanogel.

After washing via centrifugation, 10 mL of nanogels were incubated with 50 µL 0.1 M $HAuCl_4$ overnight before reduction of the gold occurs with addition of 100 µL 0.1 M $NaBH_4$ solution. Small gold domains of about 3-4 nm were formed and stabilized by the amino group of 2-aminoethyl methacrylate hydrochloride. The nanogels were used as seeds for the growth of bigger gold particles without further purification. Further growth of AuNP was carried out with formaldehyde under basic conditions. A 100 mL growth solution with a final concentration of 1 mM $HAuCl_4$, 5 mM NaBr and different amounts of seeds was prepared followed by the addition of 500 µL formaldehyde solution (37 wt%). The reduction was finally started by changing the pH to 11 through the addition of 750 µL 1 M NaOH. The reaction was very slow due to the more stable gold-bromide complexes. After 15 minutes a color change was observed but the reaction was allowed to run overnight before particles were carefully washed via centrifugation and characterized (TEM and UV-Vis spectroscopy). By simply varying the amount of seeds, AuNP with different sizes were obtained.

Loading with Doxorubicin/Pomalidomide and addition of polyelectrolyte layer

Nanogels were loaded with drugs by immersing them in solutions of Doxo and/or Poma with a final concentration of 0.25 mM of each drug and a pH adjusted to ca. 8. The nanogels were incubated overnight and the addition of the polyelectrolyte layer was carried out without further purification. After mixing, the particles were gently shaken and the mixture was incubated for 30 min. Nanogels and polyelectrolytes were mixed in a 1:1 volume ratio. The solutions of polyelectrolytes were prepared with a concentration of 1 mg/mL poly alginate, 0.5M NaCl adjusted to pH=5 and 0.5 mg/mL poly-L-arginine and 0.5 M NaCl. Thereafter, nanogels were purified by centrifugation (6 times, 2240 g for 15 min) and the supernatants were collected to calculate the loading of every drug by fluorescence spectroscopy (Varioskan Flash from Thermo Scientific) and ultra performance liquid chromatography (Acquity).

Drug release via NIR-illumination

One hundred μL of AuNG samples was placed in a 96-well transparent microplate and laser irradiation was carried out using a 808 nm fiber coupled laser diode with a maximum power of 4 W (Lumics). The spot size was chosen to iluminate the whole well at once (0.4 cm in diameter) and the power and time was adjusted to obtain the desired power density used for the experiments.

Co-culture and Live/Dead staining

Human dermal fibroblast (HDF; Invitrogen) cells were stained in suspension for 1 h, 37 °C, using Cell Tracker Blue CMF2HC (Invitrogen) at a final dilution of 1/100 in FBS free DMEM. Cells were washed and mixed 1:1 with unstained HeLa cells (a gift from Prof. Charles Lawrie, Biodonostia) and plated at a final cell number of $1x10^4$ cells/well in a 96-well plate (Ibidi μ-plate 96-well). The following day media was replaced with doxorubicin

(4 μg/mL; Sigma Aldrich) and nanogel solutions (diluted 1/25, equivalent to 4 μg/mL doxorubicin), 200 μL/well. PEGMA nanogels were incubated with cells for 2.5h, followed by washing with warm PBS (10 mM, pH 7.4) and replacement of the medium. Images were taken at various time points, after removal of nanogel solutions, using a 20× objective with DIC contrast and red and blue fluorescence channels for doxorubicin and Cell Tracker Blue (HDF cells) fluorescence respectively. A Zeiss Cell Observer microscope with AxioVision software was used.

The same cultures were used to analyze cell viability using Live/Dead (Abcam) staining after ca. 96 h. Media was replaced with 150 μl of warmed staining buffer containing 1/1000 dilutions of both "live" and "dead" fluorophores. Cells were left at 37 °C for 15 min and then imaged using a 10× objective with phase contrast and green and red fluorescence channels for "live" and "dead" staining respectively. Due to the late timepoint, HDF cells were no longer positive for Cell Tracker Blue and therefore visual comparison of cell morphology alone was used to differentiate between dead cell populations. A Zeiss Cell Observer microscope with AxioVision software was used.

Flow cytometry

Human dermal fibroblast cells were stained in suspension for 1 h, 37 °C, using Cell Tracker Blue CMF2HC at a final dilution of 1/100 in FBS free DMEM. Cells were washed and mixed 1:1 with unstained HeLa cells and plated in a 24-well plate at $5x10^4$cells/well. The following day media was replaced with doxorubicin (4 μg/ml) and nanogel solutions (diluted 1/25, equivalent to 4 μg/ml doxorubicin), 500 μL/well. PEGMA nanogels were incubated with cells for 2h30, followed by washing with warmed PBS (10 mM, pH 7.4) and replacement of the media. The following day cells were lifted up using trypsin-EDTA and

washed twice with ice-cold PBS. Samples were analysed in 1 % BSA/PBS on a BD Canto II flow cytometer using compensation. Cells were gated using the Pacific Blue channel (HeLa vs. CMF_2HC-stained HDF cells), and then the % of doxorubicin positive cells measured in the PE channel.

Cell viability; irradiation experiments

HeLa cells were plated in a 96-well TC-treated transparent plate at $5x10^4$ cells/mL, 100 µL/well. The following day media was replaced with doxorubicin (4 µg/mL) and NP solutions (diluted 1/25, equivalent to 4 µg/mL doxorubicin), 100 µL/well. NPs were left overnight with cells (approx 18 h) followed by replacement of the cell media. Individual wells were irradiated using a 808 nm fiber coupled laser diode with a maximum power of 4 W (Lumics). The spot size was chosen to illuminate the whole well at once (0.4 cm in diameter) and the power and time was adjusted to obtain the desired power density used for the experiments. The following day cell viability was analysed using the MTT assay (Roche) and absorbance measured at 550 nm, showing both non-irradiated and irradiated wells.

Transmission electron microscopy of cells

HeLa cells were grown in 60 mm diameter tissue culture treated petri dishes, $1x10^6$ cells/3 mL/dish. The following day, nanogels were added at a final dilution of 1/50, 3 ml/dish. PEGMA nanogels were incubated with cells for 2 h, followed by washing with warm PBS and replacement of the medium. The day after, cells were fixed in the dish using 2 % formaldehyde/2.5 % glutaldehyde in Sorensens buffer (initial fixation of 10 min at rt, followed by secondary fixation with fresh solution for 2 h at 4°C). Fixative was removed and cells washed using cold Sorensens buffer. A cell scrapper was used to bring the cells into suspension. Cells were embedded in 2% agar, followed by further fixation and staining

with a 1% osmodium tetraoxide solution for 1h on ice. Samples were washed with Sorensens buffer and then water, and dehydrated in an ethanol series, followed by 2 final pure ethanol and then pure acetone washes. Samples were embedded in Spurrs resin and polymerized overnight at 65 °C. One hundred nm slices were cut using an ultramicrotome and viewed using TEM (JEOL JEM-1400PLUS , 40kV - 120kV).

LPS-induced IL-6 production from J774 cells

J774 macrophages were plated in a normal tissue culture treated 96-well plate at a concentration of 2 x 10^5 cells/ml, 100 µl/well. The following day half the wells were pre-treated with LPS (Sigma Aldrich) at a final concentration of 1 µg/ml, 100 µl/well. After 1 h of LPS-stimulation, a further 100 µl of NPs (1/5 diluted, equivalent to a final pomalidomide concentration of 10 µM) were added. Controls including free pomalidomide (a final pomalidomide concentration of 10 µM), DMSO (final dilution of 1/5000 equivalent to the volume present in 10 µM pomalidomide), and pomalidomide free NPs were included. The final volume was 200 µl/well. Cells were incubated for 24 h, following which supernatants were removed and frozen for subsequent IL-6 analysis. Supernatants were analysed for IL-6 using standard sandwich ELISA with TMB substrate detection.

Angiogenesis assays

Human umbilical vein endothelial cells (HUVEC) were plated in a normal tissue culture 96-well plate at $1x10^6$ cells/ml, 100 µL/well. The following day nanogels were added at a final concentration equivalent to 10 µM pomalidomide. Cells were incubated with PEGMA nanogels for 2 h, followed by washing with warmed PBS and replacement of the media. The following day 10 µL of Geltrex (Invitrogen) was placed in the lower wells of an angiogenesis slide (Ibidi µ-slide Angiogenesis) and left to solidify at 37 °C for approximately 30 min. HUVECs, previously incubated with nanogels, were uplifted using

Trypsin-EDTA (Invitrogen), counted, and adjusted to $2x10^5$cells/ml. Fifty μL of cells were added to each well ($1x10^4$cells), taking care not to disturb the gel. Control wells without nanogel pre-incubation and with direct pomalidomide (10 μM) incubation were included. Cells were imaged approximately 6 h post seeding with a Zeiss Cell Observer microscope equipped with a x10 objective with phase contrast. AxioVision software with the "Mosaix" application was used to image the whole well (4 mm diameter).

Pomalidomide-induced cell morphological changes

HUVEC cells were plated in a 96-well plate (Ibidi μ-plate 96-well) at a concentration of $4x10^4$ cells/well, 200 μL/well. The following day media was replaced with the corresponding nanogel solution, 200 μL/well, at a final concentration equivalent to 10 μM pomalidomide. Pomalidomide-free nanogels at an equivalent concentration, and pomalidomide alone were also included. After 4 h, wells were washed with warmed PBS and fixed using a 4% formaldehyde solution in PBS. Cells were stained using DAPI (Invitrogen) and AF488-phalloidin (Invitrogen) to show the nucleus and actin fibers respectively. Images were taken using an EC Plan-Neofluar x40 oil objective with DIC contrast and filters for green (AF488-phalloidin actin staining), red (doxorubicin staining) and blue (DAPI nuclear staining) fluorescence. Cell area and aspect ratio (AR) values were calculated using ImageJ, analyzing 10 cells from 3 separate compound images composed of 9 tiles (in total ca. 30 cells/formulation).

ACKNOWLEDGMENTS

Funding is acknowledged from the European Research Council (ERC Advanced Grant#267867 Plasmaquo) and MINECO (project MAT2013-46101-R). M.S. acknowledges a co-funded PhD fellowship from University of Liverpool and CIC

biomaGUNE. We thank Dr. Andrea La Porta for his support on image representation, Dr. Luis Yate for XPS measurements and Dr. Javier Calvo for ICP-MS and UPLC measurements.

Supporting Information. Additional information about synthesis and characterization, loading and release of pomalidomide, degradation studies, in-vitro studies of nanogels without drug loading.

REFERENCES

(1) Webster, R. M. Combination Therapies in Oncology. *Nat. Rev. Drug Discov.* **2016**, *15*, 81–82.
(2) Tacar, O.; Sriamornsak, P.; Dass, C. R. Doxorubicin: An Update on Anticancer Molecular Action, Toxicity and Novel Drug Delivery Systems. *J. Pharm. Pharmacol.* **2013**, *65*, 157–170.
(3) Sun, T.; Zhang, Y. S.; Pang, B.; Hyun, D. C.; Yang, M.; Xia, Y. Engineered Nanoparticles for Drug Delivery in Cancer Therapy. *Angew. Chem. Int. Ed.* **2014**, *53*, 12320–12364.
(4) Blanco, E.; Shen, H.; Ferrari, M. Principles of Nanoparticle Design for Overcoming Biological Barriers to Drug Delivery. *Nat. Biotechnol.* **2015**, *33*, 941–951.
(5) Truong-Le, V.; Lovalenti, P. M.; Abdul-Fattah, A. M. Stabilization Challenges and Formulation Strategies Associated with Oral Biologic Drug Delivery Systems. *Adv. Drug Deliv. Rev.* **2015**, *93*, 95–108.
(6) Anselmo, A. C.; Mitragotri, S. Nanoparticles in the Clinic. *Bioeng. Transl. Med.* **2016**, *55*, 10–29.
(7) Kakwere, H.; Leal, M. P.; Materia, M. E.; Curcio, A.; Guardia, P.; Niculaes, D.; Marotta, R.; Falqui, A.; Pellegrino, T. Functionalization of Strongly Interacting Magnetic Nanocubes with (Thermo)responsive Coating and Their Application in Hyperthermia and Heat-Triggered Drug Delivery. *ACS Appl. Mater. Interfaces* **2015**, *7*, 10132–10145.
(8) Topete, A.; Alatorre-Meda, M.; Villar-Alvarez, E. M.; Carregal-Romero, S.; Barbosa, S.; Parak, W. J.; Taboada, P.; Mosquera, V. Polymeric-Gold Nanohybrids for Combined Imaging and Cancer Therapy. *Adv. Healthcare Mater.* **2014**, *3*, 1309–1325.
(9) Meng, H.; Wang, M.; Liu, H.; Liu, X.; Situ, A.; Wu, B.; Ji, Z.; Hyun Chang, C.; Nel, A. E. Use of a Lipid-Coated Mesoporous Silica Nanoparticle Platform for Synergistic Gemcitabine and Paclitaxel Delivery to Human Pancreatic Cancer in Mice. *ACS Nano* **2015**, *9*, 3540–3557.
(10) Lee, D.-E.; Koo, H.; Sun, I.-C.; Ryu, J. H.; Kim, K.; Kwon, I. C. Multifunctional

Nanoparticles for Multimodal Imaging and Theragnosis. *Chem. Soc. Rev.* **2012**, *41*, 2656–2672.

(11) Kamaly, N.; Yameen, B.; Wu, J.; Farokhzad, O. C. Degradable Controlled-Release Polymers and Polymeric Nanoparticles: Mechanisms of Controlling Drug Release. *Chem. Rev.* **2016**, *116*, 2602–2663.

(12) Kim, C. S.; Mout, R.; Zhao, Y.; Yeh, Y.-C.; Tang, R.; Jeong, Y.; Duncan, B.; Hardy, J. A.; Rotello, V. M. Co-Delivery of Protein and Small Molecule Therapeutics Using Nanoparticle-Stabilized Nanocapsules. *Bioconjug. Chem.* **2015**, *26*, 950–954.

(13) Torchilin, V. P. Multifunctional, Stimuli-Sensitive Nanoparticulate Systems for Drug Delivery. *Nat. Rev. Drug Discov.* **2014**, *13*, 813–827.

(14) Dhar S., Kolishetti N., Lippard S. J., Farokhzad, O. C. Targeted Delivery of a Cisplatinprodrug for Safer and More Effective Prostate Cancer Therapy in Vivo. *Proc. Natl. Acad. Sci. U. S. A.* **2011**, *108*, 1850–1855.

(15) Davis, M. E.; Chen, Z. G.; Shin, D. M. Nanoparticle Therapeutics: An Emerging Treatment Modality for Cancer. *Nat. Rev. Drug Discov.* **2008**, *7*, 771–782.

(16) Mackey, J. R.; Kerbel, R. S.; Gelmon, K. A.; McLeod, D. M.; Chia, S. K.; Rayson, D.; Verma, S.; Collins, L. L.; Paterson, A. H. G.; Robidoux, A.; *et al.* Controlling Angiogenesis in Breast Cancer: A Systematic Review of Anti-Angiogenic Trials. *Cancer Treat. Rev.* **2012**, *38*, 673–688.

(17) Welti, J.; Loges, S.; Dimmeler, S.; Carmeliet, P. Recent Molecular Discoveries in Angiogenesis and Antiangiogenic Therapies in Cancer. *J. Clin. Invest.* **2013**, *123*, 3190–3200.

(18) Wang, J.; Yang, Y.; Zhang, Y.; Huang, M.; Zhou, Z.; Luo, W.; Tang, J.; Wang, J.; Xiao, Q.; Chen, H.; *et al.* Dual-Targeting Heparin-Based Nanoparticles That Re-Assemble in Blood for Glioma Therapy through Both Anti-Proliferation and Anti-Angiogenesis. *Adv. Funct. Mater.* **2016**, *26*, 7873-7885.

(19) Gasparini, G. Combination of Antiangiogenic Therapy With Other Anticancer Therapies: Results, Challenges, and Open Questions. *J. Clin. Oncol.* **2005**, *23*, 1295–1311.

(20) Chu, K. F.; Dupuy, D. E. Thermal Ablation of Tumours: Biological Mechanisms and Advances in Therapy. *Nat. Rev. Cancer* **2014**, *14*, 199–208.

(21) Saxena, S.; Hansen, C. E.; Lyon, L. A. Microgel Mechanics in Biomaterial Design. *Acc. Chem. Res.* **2014**, *47*, 2426–2434.

(22) Sierra-Martin, B.; Retama, J. R.; Laurenti, M.; Fernández Barbero, A.; López Cabarcos, E. Structure and Polymer Dynamics within PNIPAM-Based Microgel Particles. *Adv. Colloid Interface Sci.* **2014**, *205*, 113–123.

(23) Kabanov, A. V.; Vinogradov, S. V. Nanogels as Pharmaceutical Carriers: Finite Networks of Infinite Capabilities. *Angew. Chem. Int. Ed.* **2009**, *48*, 5418–5429.

(24) Li, J.; Mooney, D. J. Designing Hydrogels for Controlled Drug Delivery. *Nat. Rev. Mater.* **2016**, *1*, 16071.

(25) Li, Y.; Maciel, D.; Rodrigues, J.; Shi, X.; Tomás, H. Biodegradable Polymer Nanogels for Drug/nucleic Acid Delivery. *Chem. Rev.* **2015**, *115*, 8564–8608.

(26) Austin, L. A.; MacKey, M. A.; Dreaden, E. C.; El-Sayed, M. A. The Optical, Photothermal, and Facile Surface Chemical Properties of Gold and Silver Nanoparticles in Biodiagnostics, Therapy, and Drug Delivery. *Arch. Toxicol.* **2014**, *88*, 1391–1417.

(27) Huang, X.; Jain, P. K.; El-Sayed, I. H.; El-Sayed, M. A. Plasmonic Photothermal

Therapy (PPTT) Using Gold Nanoparticles. *Lasers Med. Sci.* **2008**, *23*, 217–228.

(28) Weissleder, R. A Clearer Vision for in Vivo Imaging. *Nat. Biotechnol.* **2001**, *19*, 316–317.

(29) Dredge, K.; Marriott, J. B.; Todryk, S. M.; Muller, G. W.; Chen, R.; Stirling, D. I.; Dalgleish, A. G. Protective Antitumor Immunity Induced by a Costimulatory Thalidomide Analog in Conjunction with Whole Tumor Cell Vaccination Is Mediated by Increased Th1-Type Immunity. *J. Immunol.* **2002**, *168*, 4914–4919.

(30) Reddy, N.; Hernandez-Ilizaliturri, F. J.; Deeb, G.; Roth, M.; Vaughn, M.; Knight, J.; Wallace, P.; Czuczman, M. S. Immunomodulatory Drugs Stimulate Natural Killer-Cell Function, Alter Cytokine Production by Dendritic Cells, and Inhibit Angiogenesis Enhancing the Anti-Tumour Activity of Rituximab in Vivo. *Br. J. Haematol.* **2008**, *140*, 36–45.

(31) Lu, L.; Payvandi, F.; Wu, L.; Zhang, L. H.; Hariri, R. J.; Man, H. W.; Chen, R. S.; Muller, G. W.; Hughes, C. C. W.; Stirling, D. I.; *et al.* The Anti-Cancer Drug Lenalidomide Inhibits Angiogenesis and Metastasis via Multiple Inhibitory Effects on Endothelial Cell Function in Normoxic and Hypoxic Conditions. *Microvasc. Res.* **2009**, *77*, 78–86.

(32) Sanson, N.; Rieger, J. Synthesis of Nanogels/microgels by Conventional and Controlled Radical Crosslinking Copolymerization. *Polym. Chem.* **2010**, *1*, 965–977.

(33) Cai, T.; Marquez, M.; Hu, Z. Monodisperse Thermoresponsive Microgels of Poly(ethylene Glycol) Analogue-Based Biopolymers. *Langmuir* **2007**, *23*, 8663–8666.

(34) Guarrotxena, N.; Quijada-Garrido, I. Optical and Swelling Stimuli-Response of Functional Hybrid Nanogels: Feasible Route to Achieve Tunable Smart Core@Shell Plasmonic@Polymer Nanomaterials. *Chem. Mater.* **2016**, *28*, 1402–1412.

(35) Lutz, J. F. Polymerization of Oligo(ethylene Glycol) (Meth)acrylates: Toward New Generations of Smart Biocompatible Materials. *J. Polym. Sci. A* **2008**, *46*, 3459–3470.

(36) Hu, Z.; Cai, T.; Chi, C. Thermoresponsive Oligo(ethylene Glycol)-Methacrylate-Based Polymers and Microgels. *Soft Matter* **2010**, *6*, 2115.

(37) Lutz, J. F.; Andrieu, J.; Üzgün, S.; Rudolph, C.; Agarwal, S. Biocompatible, Thermoresponsive, and Biodegradable: Simple Preparation of "All-in-One" Biorelevant Polymers. *Macromolecules* **2007**, *40*, 8540–8543.

(38) Okada, Y.; Tanaka, F. Cooperative Hydration, Chain Collapse, and Flat LCST Behavior in Aqueous poly(N-Isopropylacrylamide) Solutions. *Macromolecules* **2005**, *38*, 4465–4471.

(39) Vihola, H.; Laukkanen, A.; Valtola, L.; Tenhu, H.; Hirvonen, J. Cytotoxicity of Thermosensitive Polymers poly(N-Isopropylacrylamide), poly(N-Vinylcaprolactam) and Amphiphilically Modified poly(N-Vinylcaprolactam). *Biomaterials* **2005**, *26*, 3055–3064.

(40) Langille, M. R.; Personick, M. L.; Zhang, J.; Mirkin, C. A. Defining Rules for the Shape Evolution of Gold Nanoparticles. *J. Am. Chem. Soc.* **2012**, *134*, 14542–14554.

(41) Bodelón, G.; Montes-García, V.; Fernández-López, C.; Pastoriza-Santos, I.; Pérez-Juste, J.; Liz-Marzán, L. M. Au@pNIPAM SERRS Tags for Multiplex Immunophenotyping Cellular Receptors and Imaging Tumor Cells. *Small* **2015**, *11*, 4149–4157.

(42) Wong, J. E.; Díez-Pascual, A. M.; Richtering, W. Layer-by-Layer Assembly of

Polyelectrolyte Multilayers on Thermoresponsive P(NiPAM- Co -MAA) Microgel: Effect of Ionic Strength and Molecular Weight. *Macromolecules* **2009**, *42*, 1229–1238.

(43) Kleinen, J.; Klee, A.; Richtering, W. Influence of Architecture on the Interaction of Negatively Charged Multisensitive poly(N-Isopropylacrylamide)-Co-Methacrylic Acid Microgels with Oppositely Charged Polyelectrolyte: Absorption vs Adsorption. *Langmuir* **2010**, *26*, 11258–11265.

(44) Casals, E.; Pfaller, T.; Duschl, A.; Oostingh, G. J.; Puntes, V. Time Evolution of the Nanoparticle Protein Corona. *ACS Nano* **2010**, *4*, 3623–3632.

(45) Zyuzin, M. V.; Honold, T.; Carregal-Romero, S.; Kantner, K.; Karg, M.; Parak, W. J. Influence of Temperature on the Colloidal Stability of Polymer-Coated Gold Nanoparticles in Cell Culture Media. *Small* **2016**, *12*, 1723–1731.

(46) Wu, W.; Shen, J.; Banerjee, P.; Zhou, S. Core-Shell Hybrid Nanogels for Integration of Optical Temperature-Sensing, Targeted Tumor Cell Imaging, and Combined Chemo-Photothermal Treatment. *Biomaterials* **2010**, *31*, 7555–7566.

(47) Meng, Z.; Wei, F.; Wang, R.; Xia, M.; Chen, Z.; Wang, H.; Zhu, M. NIR-Laser-Switched in Vivo Smart Nanocapsules for Synergic Photothermal and Chemotherapy of Tumors. *Adv. Mater.* **2016**, *28*, 245–253.

(48) Huang, G.; Gao, J.; Hu, Z.; St. John, J. V.; Ponder, B. C.; Moro, D. Controlled Drug Release from Hydrogel Nanoparticle Networks. *J. Controlled Release* **2004**, *94*, 303–311.

(49) Qian, J.; Wu, F. Thermosensitive PNIPAM Semi-Hollow Spheres for Controlled Drug Release. *J. Mater. Chem. B* **2013**, *1*, 3464–3469.

(50) Siepmann, J.; Peppas, N. A. Modeling of Drug Release from Delivery Systems Based on Hydroxypropyl Methylcellulose (HPMC). *Adv. Drug Deliv. Rev.* **2001**, *48*, 139–157.

(51) Anderson, M. E. Glutathione an Overview of Biosynthesis and Modulation. *Chem. Biol. Interact.* **1998**, *111–112*, 1–14.

(52) Wu, G.; Fang, Y.; Yang, S.; Lupton, J. R.; Turner, N. D. Recent Advances in Nutritional Sciences Glutathione Metabolism and Its Implications for Health 1. *Environ. Heal.* **2004**, *134*, 489–492.

(53) Hong, R.; Han, G.; Fernández, J. M.; Kim, B.; Forbes, N. S.; Rotello, V. M. Glutathione-Mediated Delivery and Release Using Monolayer Protected Nanoparticle Carriers. *J. Am. Chem. Soc.* **2006**, *128*, 1078–1079.

(54) Lin, C.-A. J.; Sperling, R. A.; Li, J. K.; Yang, T.-Y.; Li, P.-Y.; Zanella, M.; Chang, W. H.; Parak, W. J. Design of an Amphiphilic Polymer for Nanoparticle Coating and Functionalization. *Small* **2008**, *4*, 334–341.

(55) Wood, B. J. L. pH Controlled Hydrogen-Bonding. *Biochem. J.* **1974**, *143*, 775–777.

(56) Li Volsi, A.; Jimenez de Aberasturi, D.; Henriksen-Lacey, M.; Giammona, G.; Licciardi, M.; Liz-Marzán, L. M. Inulin Coated Plasmonic Gold Nanoparticles as a Tumor-Selective Tool for Cancer Therapy. *J. Mater. Chem. B* **2016**, *4*, 1150–1155.

(57) Zhao, Y.; Butler, E. B.; Tan, M. Targeting Cellular Metabolism to Improve Cancer Therapeutics. *Cell Death Dis.* **2013**, *4*, e532.

(58) Hu, X.-Y.; Liu, X.; Zhang, W.; Qin, S.; Yao, C.; Li, Y.; Cao, D.; Peng, L.; Wang, L. Controllable Construction of Biocompatible Supramolecular Micelles and Vesicles by Water-Soluble Phosphate pillar[5,6]arenes for Selective Anti-Cancer Drug Delivery. *Chem. Mater.* **2016**, *28*, 3778–3788.

(59) Xia, Y.; Wu, X.; Zhao, J.; Li, Z.; Ren, W.; Tian, Y.; Li, A.; Shen, Z.; Zhao, J.-T.; Wu, A. Three Dimensional Plasmonic Assemblies of AuNPs with Overall Size of Sub-200 Nm for Chemo-Photothermal Synergistic Therapy of Breast Cancer. *Nanoscale* **2016**, 18682–18692.

(60) Corral, L. G.; Haslett, P. a; Muller, G. W.; Chen, R.; Wong, L. M.; Ocampo, C. J.; Patterson, R. T.; Stirling, D. I.; Kaplan, G. Differential Cytokine Modulation and T Cell Activation by Two Distinct Classes of Thalidomide Analogues That Are Potent Inhibitors of TNF-Alpha. *J. Immunol.* **1999**, *163*, 380–386.

(61) Chanan-Khan, A. A.; Swaika, A.; Paulus, A.; Kumar, S. K.; Mikhael, J. R.; Rajkumar, S. V; Dispenzieri, A.; Lacy, M. Q. Pomalidomide: The New Immunomodulatory Agent for the Treatment of Multiple Myeloma. *Blood Cancer J.* **2013**, *3*, 1–8.

(62) Xu, Y.; Li, J.; Ferguson, G. D.; Mercurio, F.; Khambatta, G.; Morrison, L.; Lopez-Girona, A.; Corral, L. G.; Webb, D. R.; Bennett, B. L.; *et al.* Immunomodulatory Drugs Reorganize Cytoskeleton by Modulating Rho GTPases. *Blood* **2009**, *114*, 338–345.

(63) Aidoudi, S.; Bujakowska, K.; Kieffer, N.; Bikfalvi, A. The CXC-Chemokine CXCL4 Interacts with Integrins Implicated in Angiogenesis. *PLoS One* **2008**, *3*, e2657.

(64) Hosseinkhani, H.; Hosseinkhani, M.; Khademhosseini, A.; Kobayashi, H.; Tabata, Y. Enhanced Angiogenesis through Controlled Release of Basic Fibroblast Growth Factor from Peptide Amphiphile for Tissue Regeneration. *Biomaterials* **2006**, *27*, 5836–5844.

(65) Richardson, P. G.; Mark, T. M.; Lacy, M. Q. Pomalidomide: New Immunomodulatory Agent with Potent Antiproliferative Effects. *Crit. Rev. Oncol. Hematol.* **2013**, *88*, S36–S44.

Table of Contents Graphic